PROPELLER WHIRL FLUTTER CONSIDERATIONS FOR V/STOL AIRCRAFT

Wilmer H. Reed, III and Robert M. Bennett

NASA, Langley Field, Virginia

PROPELLER WHIRL CONSIDERATIONS FOR V/STOL AIRCRAFT

By Wilmer H. Reed III and Robert M. Bennett
NASA Langley Research Center

For Presentation at the CAL-TRECOM Symposium on Dynamic Loads Problems Associated With Helicopters and V/STOL Aircraft, Buffalo, New York,

June 26-27, 1963

PROPELLER WHIRL FLUTTER CONSIDERATIONS FOR V/STOL AIRCRAFT

By Wilmer H. Reed III and Robert M. Bennett

ABSTRACT

Recent studies of propeller whirl flutter conducted at the NASA Langley Research Center are reviewed and extended to encompass operating conditions peculiar to V/STOL aircraft. The extension of previous work involves consideration of angle of attack, propeller thrust, and flapping blades. Experimentally determined whirl flutter boundaries using both measured and theoretical propeller derivatives are compared with theory. As a related dynamic problem, the response of propeller-nacelle systems to random atmospheric turbulence is analyzed.

PROPELLER WHIRL FLUTTER CONSIDERATIONS FOR V/STOL AIRCRAFT

By Wilmer H. Reed III and Robert M. Bennett

INTRODUCTION

The purpose of this paper is to review recent work on propeller whirl conducted at NASA Langley Research Center, to extend these studies to include V/STOL aircraft operating conditions, and to consider a related problem - the dynamic response of a propeller-powerplant system to random atmospheric turbulence.

Until about 3 years ago the phenomenon known as propeller whirl flutter fell into the category of an interesting but academic problem of little practical concern. The possibility that a precession-type instability could develop in a flexibly mounted aircraft propeller-powerplant system was mentioned in a 1938 paper by Taylor and Browne (ref. 1) which dealt primarily with the problem of vibration isolation. Following this paper, Wright Field personnel and other groups made propeller whirl flutter calculations for new aircraft as a matter of routine. The procedure was eventually abandoned, however, when it was found that in all cases considered very large margins of safety were indicated. Then in 1960, intense interest was focused on the problem as a result of two Lockheed Electra accidents. Wind-tunnel investigations conducted in the Langley transonic dynamics tunnel indicated that if stiffness in the engine support structure was severely reduced, say through damage, propeller whirl was possible; in the undamaged condition

the aircraft had an adequate margin of safety. The solution was to modify the Electra with sufficient redundant structure to preclude a large loss of stiffness from a single failure. Because of these experiences with the Electra and the sometimes radical departures from conventional methods of installing propeller-powerplant systems - especially on V/STOL configurations - propeller whirl stability has once again become a design consideration on new propeller aircraft.

During and since the Electra investigation several generalized studies of propeller whirl have been published by the NASA. These studies show the influence of various parameters affecting the stability of a simplified representation of propeller-powerplant systems. References 2, 3, and 4 analyze the whirl stability of an isolated propeller system which is assumed to be flexibly mounted to a rigid back-up structure; more recently, unpublished experimental data have been obtained for a similar system wherein both propeller aerodynamic derivatives and whirl stability boundaries were measured. These investigations were concerned primarily with operating conditions representative of high-speed (low angle-of-attack) flight. Under such conditions it can be shown that, from the standpoint of whirl stability, the effects of mean angle of attack and thrust of the propeller are relatively unimportant and can therefore be neglected. This leaves open the question of propeller whirl stability on V/STOL aircraft during the high-thrust, high-angle-of-attack transition maneuver. Thus, one of the aims of this paper is to extend the previous generalized studies to include the effects of thrust and high mean angles of attack.

SYMBOLS

$b_{0.75R}$	propeller chord at 0.75 blade radius
B	number of propeller blades
C_m	propeller pitching-moment coefficient
$\bar{C}_m$	total pitching-moment coefficient about pitch axis of system (see eq. (8))
C_n	propeller yawing-moment coefficient
C_T	thrust coefficient, $\frac{T}{\rho\left(\frac{\Omega}{2\pi}\right)^2(2R)^4}$
C_Y	propeller side-force coefficient
C_Z	propeller vertical-force coefficient
e	offset of blade hinge axis
$h_{\theta\bar{v}}, h_{\theta\bar{w}}$	response in θ due to unit impulse in $\bar{v}$ and $\bar{w}$, respectively
H	moment-of-inertia ratio, $\frac{\pi I_x}{I_y}$
$H_{\theta\bar{v}}, H_{\theta\bar{w}}$	frequency-response functions giving response in θ to unit sinusoidal inputs in $\bar{v}$ and $\bar{w}$, respectively
I_x	mass moment of inertia of propeller about axis of rotation
I_y	mass moment of inertia of propeller-powerplant system about pitch axis
J	propeller advance ratio, $\frac{\pi U}{\Omega R}$
k, k_θ	reduced-frequency parameters, $k = \frac{\omega R}{U}$, $k_\theta = \frac{\omega_\theta R}{U}$
l	distance from plane of propeller to pitch axis
L	scale of atmospheric turbulence
R	propeller radius
S_θ	rotational stiffness of powerplant mount about pitch axis

t, τ, T time

$u(t)$, $v(t)$, $w(t)$ longitudinal, lateral, and vertical components of turbulence velocity

$\bar{v}$, $\bar{w}$ flow angles due to turbulence, $\bar{v} = \frac{V}{U}$, $\bar{w} = \frac{W}{U}$

$\overline{V}(\omega)$, $\overline{W}(\omega)$ Fourier transforms of $v(t)$ and $w(t)$, respectively

α angle of attack of propeller

β geometric blade angle at 0.75R measured from propeller plane of rotation

ζ viscous damping ratio

θ, ψ geometric pitch and yaw angles

θ_g, ψ_g effective pitch and yaw angles in turbulent flow (see eq. (9))

$\Theta(\omega)$ Fourier transform of $\theta(t)$

κ density-inertia ratio, $\frac{\pi\rho R^5}{I_y}$

ρ air density

σ^2 mean-square value of turbulence velocity component

τ nondimensional time, $\frac{Ut}{R}$

Φ_θ, $\Phi_{\theta w}$ power spectra and cross spectra, where subscripts denote the associated time histories

Ω propeller rotational frequency

ω circular frequency

Subscripts:

q	differentiation with respect to θ'
r	differentiation with respect to ψ'
θ	pitch direction
ψ	yaw direction

Primes denote differentiation with respect to τ.

Partial derivatives are denoted by double subscripts; for example, $C_{m_\theta} = \frac{\partial C_m}{\partial \theta}$, $C_{m_q} = \frac{\partial C_m}{\partial q}$, and so forth.

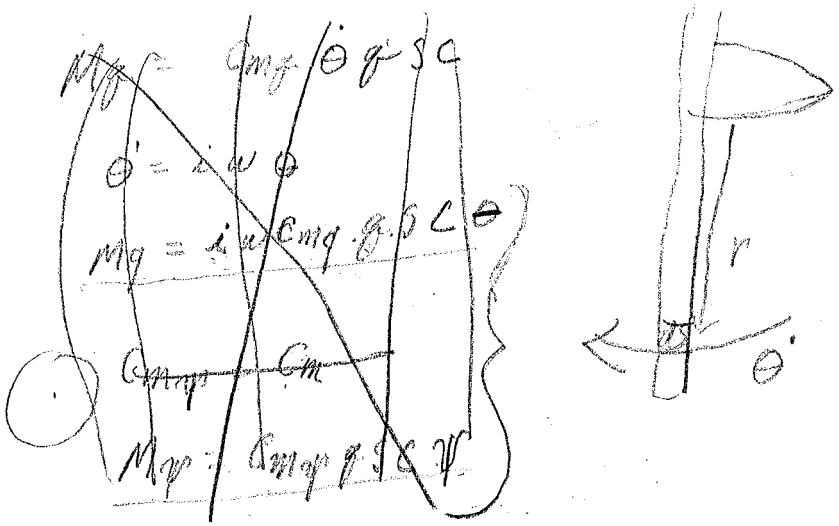

$$\frac{r\dot{\theta}}{r\Omega} = \frac{w}{\Omega}\theta$$

$$dM_{\dot{\theta}} = \frac{r\dot{\theta}}{r\Omega}(r\Omega)^2 \rho\, ds$$

$$M_{\dot{\theta}} = K\frac{\dot{\theta}}{\Omega} D^4 \Omega^2 \rho$$

$$M_{\dot{\theta}} = KD^4 \rho \dot{\theta}\Omega = (KD^3\rho) D\dot{\theta}\Omega$$

DYNAMIC SYSTEM

A schematic diagram of the idealized propeller-powerplant system to be considered in this paper is shown in figure 1. The system is mounted on two springs, S_θ and S_ψ, located a distance l behind the plane of the propeller. These springs permit small angular deflections θ and ψ of the propeller axis from its equilibrium position which is inclined at an arbitrary angle α from the free stream. Damping, which in an actual system would be introduced by hysteresis or friction in the mounts, fuel lines, electrical conduits, etc., is here simulated by equivalent viscous damping ζ_ψ and ζ_θ. Other variables shown in the figure are the airstream velocity U and, the rotational speed of the propeller Ω.

MECHANISM OF WHIRL FLUTTER

Let us briefly review some basic aspects of propeller whirl flutter. The dynamic behavior of a propeller-powerplant system is governed by an interaction of the aerodynamic and gyroscopic moments on the rotating propeller, the inertia forces of the propeller-powerplant system, and the damping and elastic forces in the mount structure. If the propeller is replaced by an equivalent nonrotating mass and the aerodynamic forces are neglected, natural vibrations of the system about the pitch axis can occur independently of those about the yaw axis. On the other hand, if the propeller is replaced by an equivalent rotating mass, or flywheel, the associated gyroscopic moments prevent the occurrence of independent motions in

either pitch or yaw so that the natural vibrations of the system are characterized by a precession or wobbling motion of the rotation axis. The variation of these so-called "precession" modes with rotational speed of the flywheel is illustrated in figure 2 for a system having symmetrical stiffness in pitch and yaw. Note that as the angular velocity Ω of the flywheel is increased, the frequency of one mode increases while that of the other decreases. As illustrated by the sketches on the right of the figure, the flywheel shaft follows a circular path for each mode. For the higher frequency mode the direction of precession is the same as that of rotation and is thus referred to as the "forward" mode; alternatively, for the lower frequency mode the direction of precession is opposite that of rotation and is referred to as the "backward" mode. These modes can only be stable, for there is no mechanism by which the flywheel can add energy to the system.

Let the flywheel be replaced by a propeller having the same angular momentum. Now when precession occurs, aerodynamic forces and moments are generated due to angle-of-attack changes on blade elements of the propeller. These forces and moments are governing factors that determine whether the precession modes of a given system will damp out following a disturbance, such as a gust, or will build up with time until the structure fails or its motion becomes limited by the presence of nonlinearities. It has been found that on conventional propellers whirl flutter invariably occurs in the backward whirl mode.

The generalized propeller whirl studies of references 2, 3, and 4 show trends for many parameters that affect the stability of the system shown in figure 1. It is beyond the scope of this paper to summarize these trends; however, one type of stability-boundary plot is particularly enlightening and will be discussed with the aid of figure 3. This figure shows the pitch and yaw stiffness required for stability for three values of structural damping (the physical properties of the system treated are tabulated in reference 3 under system 2A with $J = 1.8$). Both whirl-flutter and static-divergence boundaries are presented. An important feature shown, which appears to be characteristic of most propeller whirl systems, is the pronounced sensitivity of the stability boundaries to small changes in structural damping when the damping is near zero. Thus, to assume zero structural damping for a propeller system, as is often done as a measure of conservatism in conventional wing flutter analyses, would probably lead to an unduly low estimate of the whirl flutter speed. Note also that the shapes of the whirl boundaries are likewise highly dependent on damping.

COMPARISON OF THEORY AND EXPERIMENT

To enable a better evaluation of theoretical methods for predicting whirl flutter, some experimental data have been obtained on a model which closely resembles the idealized mathematical model treated in references 2, 3, and 4. The model is shown in figure 4 and its physical properties are given in table I under

system 1. These data, obtained by Bland and Bennett (ref. 5), include measurements of both static aerodynamic propeller derivatives and whirl-flutter boundaries. Typical results from the study are presented in figure 5, which shows the viscous damping required to prevent flutter plotted against a nondimensional velocity ratio.

The calculated stability boundaries shown for comparison are based on three sets of propeller aerodynamic derivatives: theoretical derivatives evaluated by the methods of Ribner (ref. 6) and Houbolt and Reed (ref. 3), and the actual derivatives that were measured on the model (the damping derivative C_{m_q} was not measured, so it was calculated by the method of ref. 6).

It can be seen from the figure that the calculations based on measured derivatives are in excellent agreement with the experimental data, while those based on theoretical derivatives predict somewhat lower flutter velocities than were observed. Similar comparisons between theory and experiment were also indicated for other values of such system parameters as advance ratio, inertia, and pivot-point location.

V/STOL TRANSITION

The propeller of a V/STOL vehicle, such as a tilt-wing aircraft, will undergo large changes in thrust and mean angle of attack during transition from hovering to high-speed flight. Since previous generalized studies (refs. 2, 3, and 4) have been concerned primarily with the high-speed flight regime where angle-of-attack and thrust effects are known to have a negligible influence on whirl stability,

it is of interest to explore the possibility of encountering propeller whirl during low-speed transition maneuvers. For this purpose some whirl stability calculations have been made, utilizing experimental static propeller derivatives obtained by Yaggy and Rogallo in the Ames 40- by 80-foot tunnel for high angle-of-attack and thrust conditions typical of VTOL operations. (See ref. 7, propeller 1.) These derivatives, which were determined graphically from data presented in reference 7, are shown in figure 6 of the present report. It should be noted that since the damping derivative C_{m_q} was not measured in reference 7 it has been necessary to use theoretically determined values and make the assumption that angle-of-attack effects on C_{m_q} are negligible. The system considered in these calculations is identified in table I as system 2.

Figure 7 indicates the effect of angle of attack on the stiffness required to prevent flutter. The curves have been normalized with respect to the stiffness required at zero angle of attack. Little effect of angle of attack is noted for $\beta = 13.0^\circ$, which corresponds to a low thrust condition ($C_T = 0$ at $\alpha = 0$); at $\beta = 36.5^\circ$, which represents a high thrust condition ($C_T = 0.24$ at $\alpha = 0$), a moderate stabilizing effect is present.

The effects of thrust coefficient for angles of attack up to 30° are presented in figure 8 for several values of advance ratio. The figure indicates, as has been shown in previous studies, that propeller thrust effects are negligible for advance ratios representative of high-speed flight ($J > 2.0$). At low forward speeds during

transition, however, thrusting propellers are seen to have a destabilizing influence on whirl flutter.

The combined effects of thrust and angle of attack on the whirl flutter during a hypothetical transition maneuver are illustrated in figure 9. The assumed variations of α and C_T with forward velocity are given on the left-hand side of the figure and the associated flutter boundary, in the form of damping required to prevent flutter, is on the right. (Velocity was determined by assuming $\omega_\theta R = 76.8$ so that $V = \frac{76.8}{k}$ ft/sec.) Shown for comparison is the flutter boundary computed on the basis of $C_T = 0$ and $\alpha = 0$. Although the overall effects of thrust and angle of attack are slightly destabilizing, the large margin of stability at low forward speeds would seem to indicate that propeller whirl problems would not occur during the transition maneuver. It should be pointed out that these conclusions are based on the assumption that C_{m_q} is essentially independent of angle-of-attack changes during transition.

FLAPPING HINGES

Propellers with blades hinged to permit flapping in a plane perpendicular to the propeller rotation axis have been proposed for V/STOL applications. Some unpublished data obtained on such a system by E. F. Baird of Grumman Aircraft Engineering Corporation indicated a possible occurrence of whirl flutter in the forward mode as well as the backward mode which is typical of fixed blade designs. In an effort to gain further insight into the problem, we have

conducted a brief exploratory wind-tunnel investigation on a simple model.

The model, shown in figure 10, consists of a windmilling propeller attached to a rod which has freedom to pitch and yaw about a set of gimbal axes. The system has symmetrical stiffness that can be controlled by varying tension in a spring connected axially at the other end of the rod. Each propeller blade is attached to the hub by means of two pins. When both pins are in position the blade is fixed; when one of the pins is removed the other pin becomes a hinge about which the blade is free to flap. (See fig. 10.) In this way the blades can be hinged at either 0.08 or 0.13 of the propeller radius from the spin axis. Other physical properties of the model, identified herein as system 3, may be found in table I.

Whirl-flutter boundaries for the flapping-blade and fixed-blade conditions are presented in figure 11. Both forward and backward whirl instabilities were encountered. The system became unstable in the backward mode for the fixed blade and the 0.13R hinge offset, but instability developed in the forward mode with the smaller hinge offset of 0.08R. Note that for flutter in the backward mode blade flapping had a significant stabilizing influence; just the opposite conclusions are indicated for flutter in the forward mode. In addition to frequency differences (backward whirl occurs at low frequency, forward whirl at high frequency), the two modes behaved differently in other respects. Whereas backward whirl instability was accompanied by divergent motions as predicted by linear theory, forward whirl instability was characterized by amplitude limited motions which could be excited when the disturbing force exceeded a threshold level. The

implication to be drawn from these preliminary studies is that blade flapping, and possibly blade flexibility, can have either strong stabilizing or destabilizing influences on propeller whirl flutter. Additional research is required to further delineate these aspects of the problem.

RESPONSE TO RANDOM ATMOSPHERIC TURBULENCE

Previous sections of the paper have dealt with factors that affect the stability of propeller-powerplant systems. A related problem of interest in connection with dynamic loads and fatigue is the response of such systems to gusts and turbulence in the atmosphere. These loads may be significant even though the system is operating well on the stable side of its whirl-flutter boundary.

The gust response problem and a method of analysis is illustrated in figure 12. The free-stream velocity is represented by a mean velocity U, upon which is superimposed unsteady velocity components $u(t)$, $v(t)$, and $w(t)$. These time-dependent velocities produce unsteady forces and moments on the propeller which in turn cause pitch and yaw deflections, $\theta(t)$ and $\psi(t)$, of the flexibly mounted system. If turbulence is considered to be a stationary random process, a solution can be obtained for the response of the system to multiple random inputs $u(t)$, $v(t)$, and $w(t)$. This requires specifications of the power spectra and cross spectra of the inputs, together with a set of frequency-response functions which define the response of the system to sinusoidal variations of the gust velocity components. If the turbulence is considered to be isotropic, the cross-spectrum terms become zero and the equation for the power spectrum of response of the system in, say, pitch can be written

$$\Phi_\theta = \Phi_w\left[\left|H_{\theta w}\right|^2 + \left|H_{\theta v}\right|^2\right]$$

where Φ_w is the power spectrum of the v and w components of turbulence and $H_{\theta v}$ and $H_{\theta w}$ represent the response in pitch to unit-amplitude sinusoidal v and w inputs. It is assumed that $H_{\theta u} = 0$. (For derivation of equations, see appendix.) A graphical indication of the way in which typical power spectra and frequency-response functions for a system might vary with frequency is also shown in figure 12. It should be mentioned that the frequency-response function $H_{\theta v}$ - that is, the response in a vertical plane due to a horizontal gust input - is a measure of the aerodynamic and gyroscopic coupling produced by the propeller. The two peaks in the frequency-response curve occur at the backward and forward whirl frequencies.

For purposes of illustration, figure 13 shows the calculated response to random turbulence for system 1, whose whirl-flutter boundary was presented in figure 5. The conditions chosen for these calculations are $\frac{U}{R\omega_\theta} = 2.0$ and $\zeta = .05$, which, as can be seen in figure 5, fall well within the stable region since the damping required for stability at this $\frac{U}{R\omega_\theta}$ value is $\zeta = 0.002$. The analytical expression for the turbulence spectrum assumed in the calculations is the approximation given in reference 8 for isotropic turbulence at high frequencies:

$$\Phi_w = \frac{0.521\sigma^2}{L^{3/2}\left(\frac{\omega}{U}\right)^{5/3}}$$

where σ^2 is the mean-square value of w and L in the scale of turbulence, assumed here to be 5,000 feet. It was also necessary to specify a propeller radius, which was taken to be R = 6.75 feet for these calculations.

The solid curve in figure 13 represents the power spectrum of the response of the system in pitch. (Since the system was assumed to have symmetrical stiffness, this curve also represents the response in yaw.) The dashed curve shown for comparison indicates the quasi-static response, that is, the response calculated by neglecting the time-dependent inertia, gyroscopic, and damping forces. The relative magnitudes of these two curves at a given frequency indicates the amplification of response due to dynamics of the system. As would be expected, the amplification is highest at frequencies corresponding to the natural whirl modes and becomes sharply attenuated at higher frequencies.

CONCLUDING REMARKS

This paper has examined some potential problem areas relating to propeller whirl response and flutter on V/STOL aircraft. From limited studies presented herein on highly idealized systems the following general conclusions are indicated:

1. Calculated whirl-flutter boundaries based on theoretical propeller derivatives are in reasonable agreement with experimental data; those based on measured derivatives are in excellent agreement with experiment.

2. For flight conditions representative of transition maneuvers, the effects of large angle of attack and large thrust coefficient are relatively unimportant from the standpoint of propeller whirl stability.

3. Flapping propeller blades can have significant stabilizing or destabilizing influences on propeller whirl and make possible the occurrence of flutter in the forward whirl mode.

4. Power-spectral-density techniques offer a convenient means of analyzing the response of propeller-powerplant systems to random atmospheric turbulence.

APPENDIX

DERIVATION OF EQUATIONS FOR RESPONSE OF PROPELLER-NACELLE TO RANDOM ATMOSPHERIC TURBULENCE

Response Equations

The problem considered is that of calculating the dynamic response of a propeller-nacelle system to random fluctuations of the free-stream velocity. The response quantities of interest are the pitch and yaw deflections of the system which is assumed to be flexibly mounted to a rigid backup structure.

Consider the free-stream velocity to be represented by the vector addition of the flight velocity U and time-varying gust velocities $u(t)$, $v(t)$, and $w(t)$ as is shown in figure 12. It will be assumed that the gust components act uniformly over the propeller disk and that the response induced by the $u(t)$ component is negligible. Since the analytical procedures are the same for both pitch and yaw, only the pitch response will be treated.

The pitch angle $\theta(t)$ of the system can be expressed in terms of arbitrary time variations of flow angularity due to gusts, $\bar{v}(t) = \frac{v(t)}{U}$ and $\bar{w}(t) = \frac{w(t)}{U}$, by means of the superposition integral

$$\theta(t) = \int_{-\infty}^{\infty} \bar{v}(t) h_{\theta\bar{v}}(t - \tau)\,d\tau + \int_{-\infty}^{\infty} \bar{w}(t) h_{\theta\bar{w}}(t - \tau)\,d\tau \quad (1)$$

where $h_{\theta\bar{v}}$ is the response in θ to a unit impulse in $\bar{v}$ and similarly $h_{\theta\bar{w}}$ is the response to a unit impulse in $\bar{w}$. Note that the function $h_{\theta\bar{v}}$ is a coupling term which describes the response in a vertical plane associated with gusts in the horizontal plane. This term is a result of the aerodynamic and gyroscopic coupling moments on the propeller.

The gust components considered herein are random functions which cannot be expressed explicitly in terms of time, as is required in equation (1). If equation (1) is rewritten in terms of frequency rather than time, however, the problem becomes readily amenable to analysis by power spectral density techniques. (See ref. 8.)

The Fourier transform of $\theta(t)$ is defined as

$$\Theta(\omega) = \lim_{T \to \infty} \int_{-T}^{T} \theta(t) e^{-i\omega t}\,dt \quad (2)$$

Substitution of equation (1) for $\theta(t)$ into equation (2) gives

$$\Theta(\omega) = \bar{V}(\omega) H_{\theta\bar{v}}(\omega) + \bar{W}(\omega) H_{\theta\bar{w}}(\omega) \quad (3)$$

where $\bar{V}(\omega)$ and $\bar{W}(\omega)$ are Fourier transforms of the flow angles $\bar{v}(t)$ and $\bar{w}(t)$, respectively, and $H_{\theta\bar{v}}(\omega)$ and $H_{\theta\bar{w}}(\omega)$ are frequency-response functions which describe the pitch response of the system to unit sinusoidal inputs in $\bar{v}$ and $\bar{w}$.

The power spectrum of the response $\Phi_\theta(\omega)$ is related to its Fourier transform by the expression

$$\Phi_\theta(\omega) = \lim_{T \to \infty} \frac{1}{2\pi T} \Theta(\omega)\Theta^*(\omega) \tag{4}$$

where Θ^* is the complex conjugate of Θ. From equation (3) the spectrum of the response then follows as

$$\Phi_\theta(\omega) = \lim_{T \to \infty} \frac{1}{2\pi T} (\bar{V}H_{\theta\bar{v}} + \bar{W}H_{\theta\bar{w}})(\bar{V}^*H^*_{\theta\bar{v}} + \bar{W}^*H^*_{\theta\bar{w}})$$

$$= \Phi_{\bar{v}}\left|H_{\theta\bar{v}}\right|^2 + \Phi_{\theta\bar{w}}\left|H_{\theta\bar{w}}\right|^2 + \Phi_{\bar{v}\bar{w}}H_{\theta\bar{v}}H^*_{\theta\bar{w}} + \Phi_{\bar{w}\bar{v}}H_{\theta\bar{w}}H^*_{\theta\bar{v}} \tag{5}$$

where $\Phi_{\bar{v}\bar{w}}$ and $\Phi_{\bar{w}\bar{v}}$ are the cross spectra between $\bar{v}$ and $\bar{w}$ components of turbulence. Henceforth it will be assumed that the turbulence is isotropic so that the following simplifications can be introduced

$$\Phi_{\bar{v}} = \Phi_{\bar{w}}$$

$$\Phi_{\bar{v}\bar{w}} = \Phi_{\bar{w}\bar{v}} = 0$$

Thus equation (5) reduces to

$$\Phi_\theta = \Phi_{\bar{w}}\left[\left|H_{\theta\bar{v}}\right|^2 + \left|H_{\theta\bar{w}}\right|^2\right] \tag{6}$$

Frequency-Response Functions

The frequency-response functions in equation (6) can be derived by including a sinusoidal gust forcing function on the right-hand side of the equations of motion for the system. For convenience the two-degree-of-freedom symmetrical system considered in reference 2 will be treated as an example. With slight modifications of the notation in reference 2, the equations of motion for the propeller-nacelle system with gust terms included become

$$\theta'' + \frac{H}{J}\psi' + 2\zeta_\theta k_\theta \theta' + k_\theta^2 \theta = \left(\overline{C}_{m_\theta}\theta_g + \overline{C}_{m_q}\theta'_g + \overline{C}_{m_\psi}\psi_g + \overline{C}_{m_r}\psi'_g\right)$$

$$\psi'' - \frac{H}{J}\theta' + 2\zeta_\psi k_\psi \psi' + k_\psi^2 \psi = \left(\overline{C}_{m_\theta}\psi_g + \overline{C}_{m_q}\psi'_g - \overline{C}_{m_\psi}\theta_g - \overline{C}_{m_r}\theta'_g\right) \tag{7}$$

where a viscous-type damping in the mount system has been assumed. The aerodynamic coefficients with bar superscripts denote the total moments about the elastic axes of the system due to aerodynamic forces and moments on the propeller and are defined as follows:

$$\overline{C}_{m_\theta} = \kappa\left(C_{m_\theta} - \frac{l}{2R} C_{Z_\theta}\right)$$

$$\overline{C}_{m_\psi} = \kappa\left(C_{m_\psi} - \frac{l}{2R} C_{Z_\psi}\right)$$

$$\overline{C}_{m_q} = \kappa\left[C_{m_q} - \frac{l}{R}\left(\frac{1}{2} C_{Z_q} + C_{m_\theta} - \frac{l}{2R} C_{Z_\theta}\right)\right]$$

$$\overline{C}_{m_r} = \kappa\left[C_{m_r} - \frac{l}{2R} C_{Z_r} - \frac{l}{R}\left(C_{m_\psi} - \frac{l}{2R} C_{Z_\psi}\right)\right] \tag{8}$$

The terms θ_g and ψ_g in equation (7) represent the resultant airstream angles at the propeller associated with the combined effects of angular deflections of the system plus gust velocities.

$$\theta_g = \theta - \bar{w}$$
$$\psi_g = \psi + \bar{v} \tag{9}$$

Assume a simple harmonic variation in the $\bar{w}$ gust component and zero disturbance in the $\bar{v}$ component. The forcing function and the resulting response then become

$$\bar{w} = \bar{w}_o e^{ik\tau}$$
$$\bar{v} = 0$$
$$\theta = \theta_o e^{ik\tau}$$
$$\psi = \psi_o e^{ik\tau} \tag{10}$$

where $k = \frac{\omega R}{U}$ is the nondimensional driving frequency and $\tau = \frac{Ut}{R}$ is the nondimensional time variable.

Equations (9) and (10) substituted into equation (7) lead to the following pair of simultaneous equations for θ_o and ψ_o:

$$(A + iB)\theta_o + (C + iD)\psi_o = (E + iF)\bar{w}_o$$
$$-(C + iD)\theta_o + (A + iB)\psi_o = (-C + iK)\bar{w}_o \tag{11}$$

where with the assumption of structural symmetry $k_\theta = k_\psi$ and $\zeta_\theta = \zeta_\psi = \zeta$, the coefficients in equation (11) are

$$A = k_\theta^2 - k^2 - \bar{C}_{m_\theta}$$

$$B = (2\zeta k_\theta - \bar{C}_{m_q})k$$

$$C = -\bar{C}_{m_\psi}$$

$$D = \frac{H}{J} - \bar{C}_{m_r}$$

$$E = -\bar{C}_{m_\theta}$$

$$F = -\bar{C}_{m_q}k$$

$$K = \bar{C}_{m_r}k \tag{12}$$

The frequency-response functions for θ and ψ are by definition

$$H_{\theta\bar{w}} = \frac{\theta_o}{\bar{w}_o}$$

$$H_{\psi\bar{w}} = \frac{\psi_o}{\bar{w}_o} \tag{13}$$

But since the system under consideration is symmetrical in pitch and yaw the second of equations (13) can be written

$$H_{\psi\bar{w}} = H_{\theta\bar{v}} \tag{14}$$

Thus, from a simultaneous solution of equations (11) for $\frac{\theta_o}{\bar{w}_o}$ and $\frac{\psi_o}{\bar{w}_o}$ the frequency-response functions may be expressed in the form of the following complex ratios:

$$H_{\theta\bar{w}} = \frac{A_1 + iB_1}{\Delta_R + i\,\Delta_I}$$

$$H_{\theta\bar{v}} = \frac{A_2 + iB_2}{\Delta_R + i\,\Delta_I} \tag{15}$$

or

$$H_{\theta\bar{w}}{}^2 = \frac{A_1{}^2 + B_1{}^2}{\Delta_R{}^2 + \Delta_I{}^2}$$

$$H_{\theta\bar{v}}{}^2 = \frac{A_2{}^2 + B_2{}^2}{\Delta_R{}^2 + \Delta_I{}^2} \tag{16}$$

where

$$A_1 = AE + C^2 - BF + DK$$

$$B_1 = BE + CD + AF - CK$$

$$A_2 = CE - AC - BK - DF$$

$$B_2 = DE - BC + AK + CF$$

$$\Delta_R = A^2 + C^2 - B^2 - D^2$$

$$\Delta_I = 2AB + 2CD$$

With these frequency-response functions and an assumed form of the spectrum of turbulence (see ref. 8, for example) the spectrum of resulting response of the system can be calculated by means of equation (6).

REFERENCES

1. Taylor, E. S., and Browne, K. A.: Vibration Isolation of Aircraft Power Plants. Jour. Aero. Sci., vol. 6, no. 2, Dec. 1938, pp. 43-49.

2. Reed, Wilmer H., III, and Bland, Samuel R.: An Analytical Treatment of Aircraft Propeller Precession Instability. NASA TN D-659, 1961.

3. Houbolt, John C., and Reed, Wilmer H., III: Propeller-Nacelle Whirl Flutter. Jour. Aerospace Sci., vol. 29, no. 3, 1962, pp. 333-346.

4. Sewall, John L.: An Analytical Trend Study of Propeller Whirl Instability. NASA TN D-996, 1962.

5. Bland, Samuel R., and Bennett, Robert M.: Wind-Tunnel Measurement of Propeller Whirl-Flutter Speeds and Static-Stability Derivatives and Comparison With Theory. NASA TN D-1807, 1963.

6. Ribner, Herbert S.: Propellers in Yaw. NACA Rep. 820, 1945.

7. Yaggy, Paul F., and Rogallo, Vernon L.: A Wind-Tunnel Investigation of Three Propellers Through an Angle-of-Attack Range From 0° to 85°. NASA TN D-318, 1960.

8. Houbolt, John C., Steiner, Roy, and Pratt, Kermit G.: Flight Data Considerations of the Dynamic Response of Airplanes to Atmospheric Turbulence. Presented to the Structures and Materials Panel and to the Flight Mechanics Panel, AGARD, Paris, France, July 3-13, 1962.

TABLE I.- SUMMARY OF SYSTEM CHARACTERISTICS.

	System		
	1	2	3
$\frac{I_x}{I_y}$	0.135	0.135	0.583
$\frac{b_{0.75R}}{R}$	.216	.196	.160
$\frac{l}{R}$	.346	.350	.250
κ	.0466	.0504	1.78
B	4	3	4
J	2.66	varies	1.1
S_θ/S_ψ	1.0	1.0	1.0

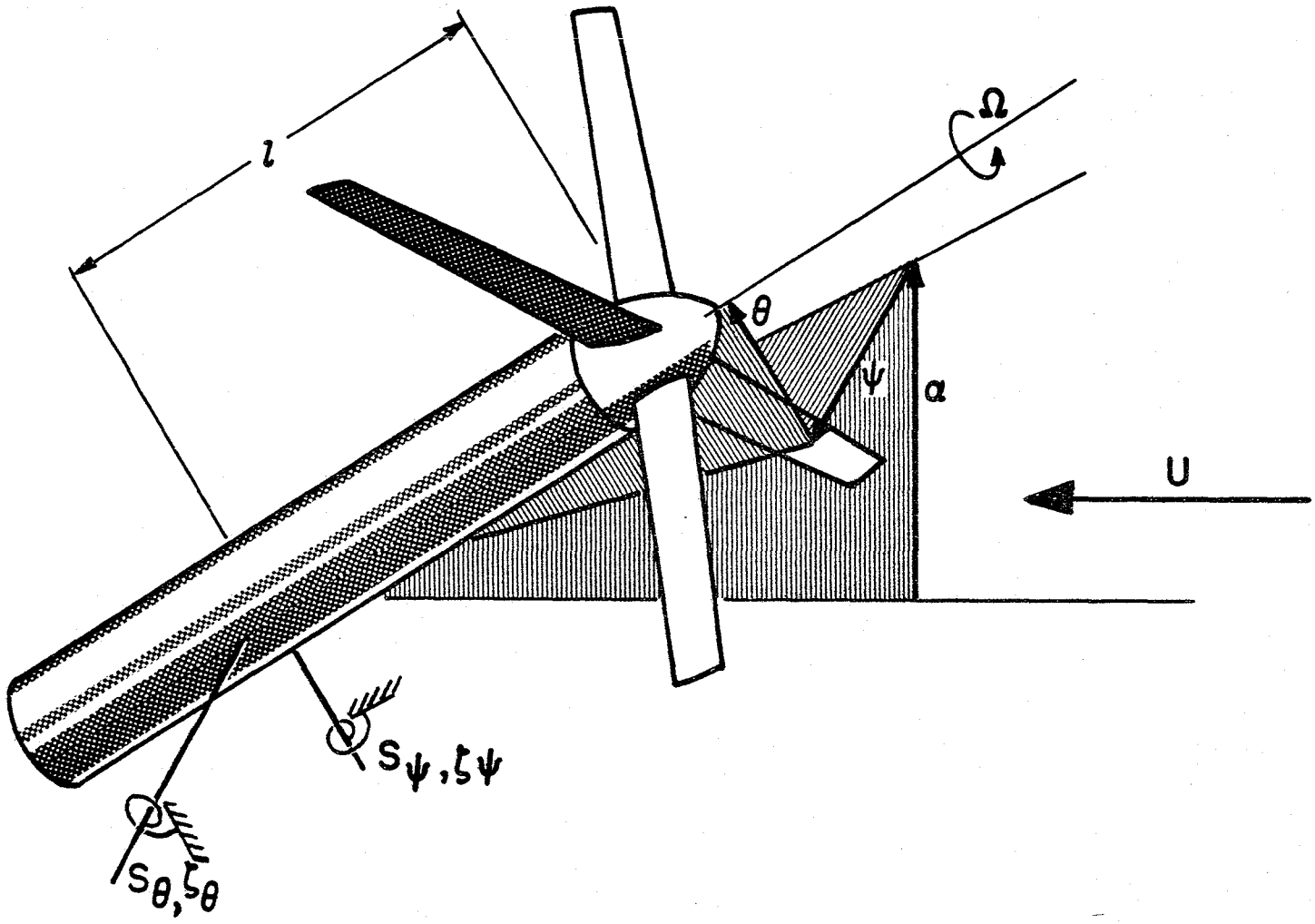

NASA

Figure 1.- System considered.

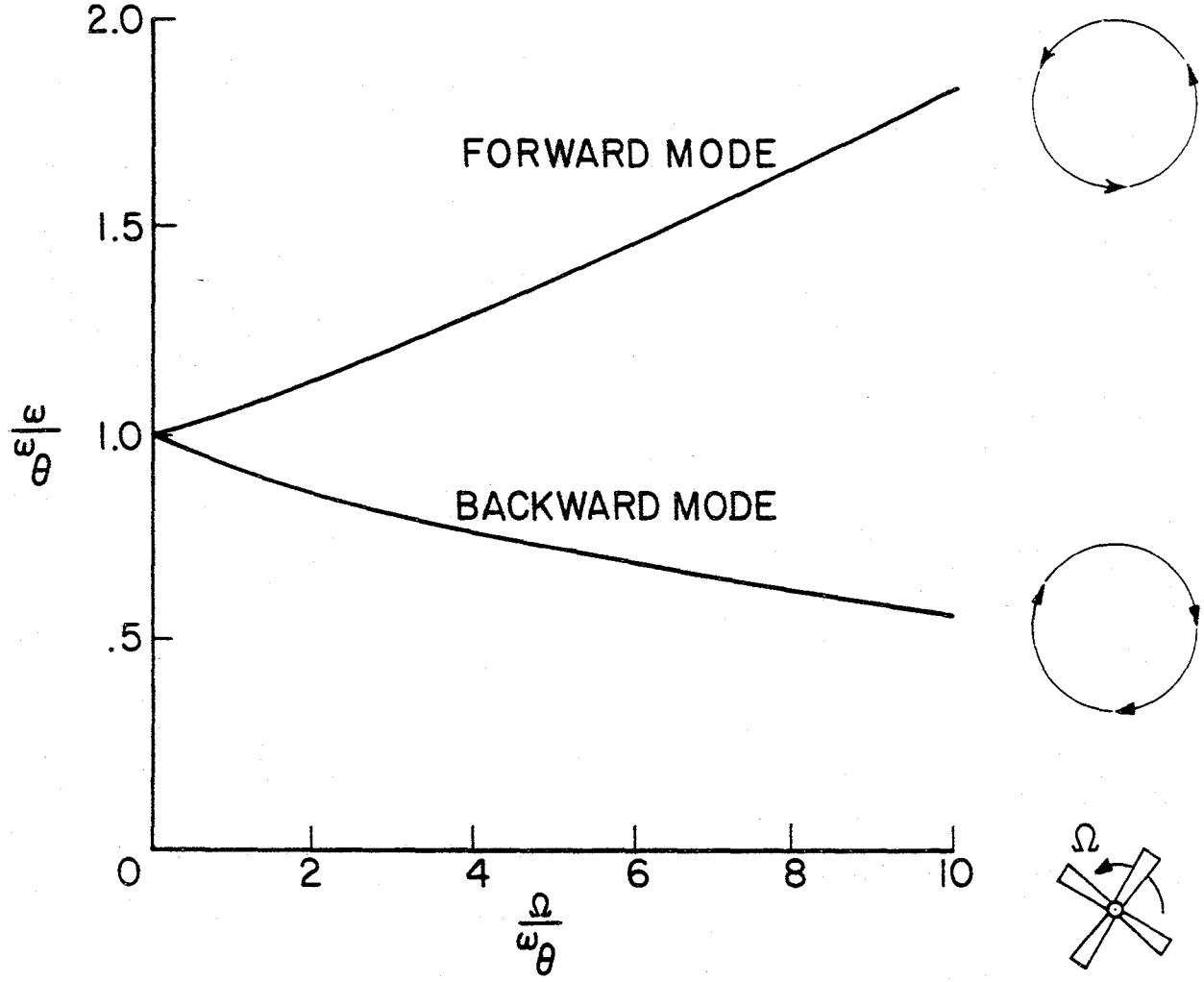

NASA

Figure 2.- Natural precession frequencies $\left(\omega_\theta = \omega_\psi\right)$.

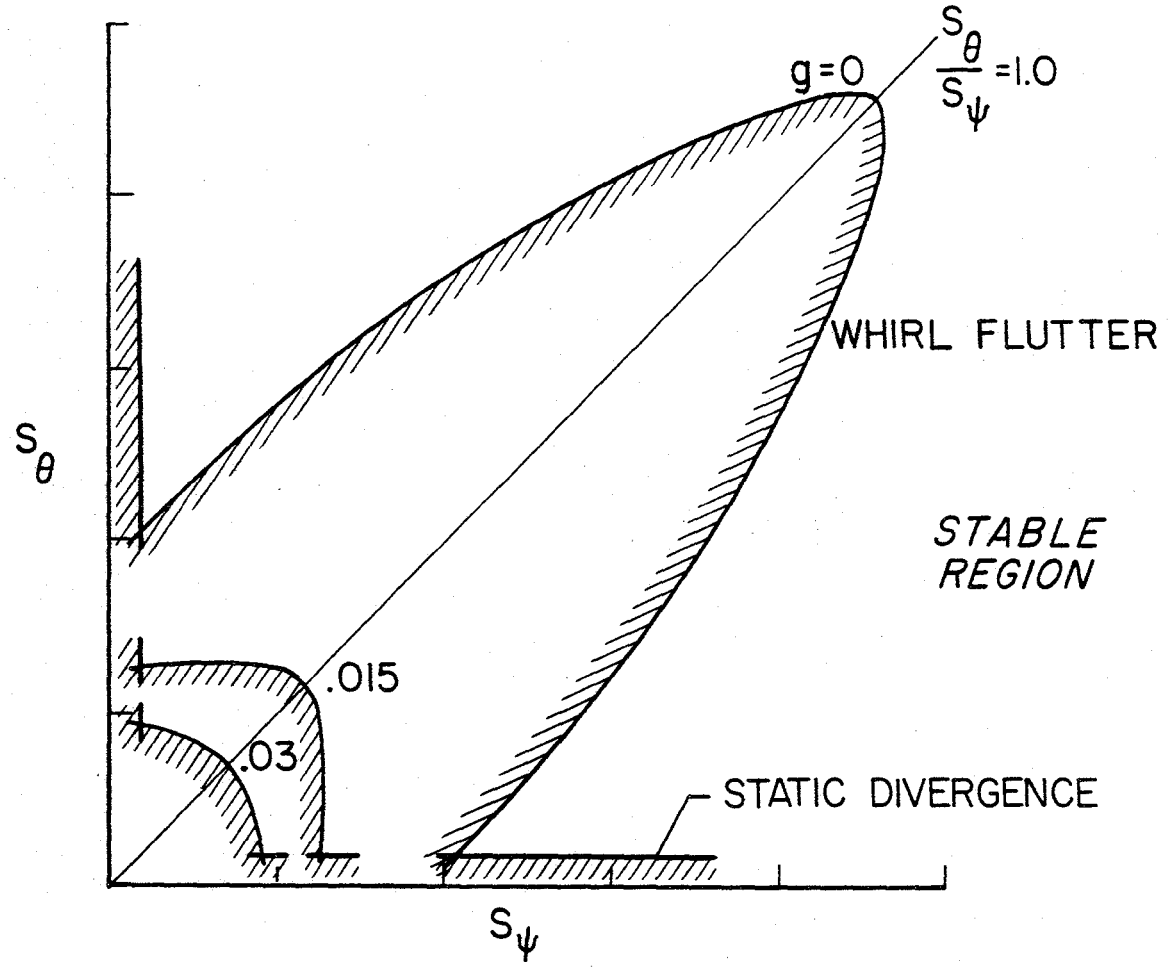

NASA

Figure 3.- Pitch and yaw stiffness required.

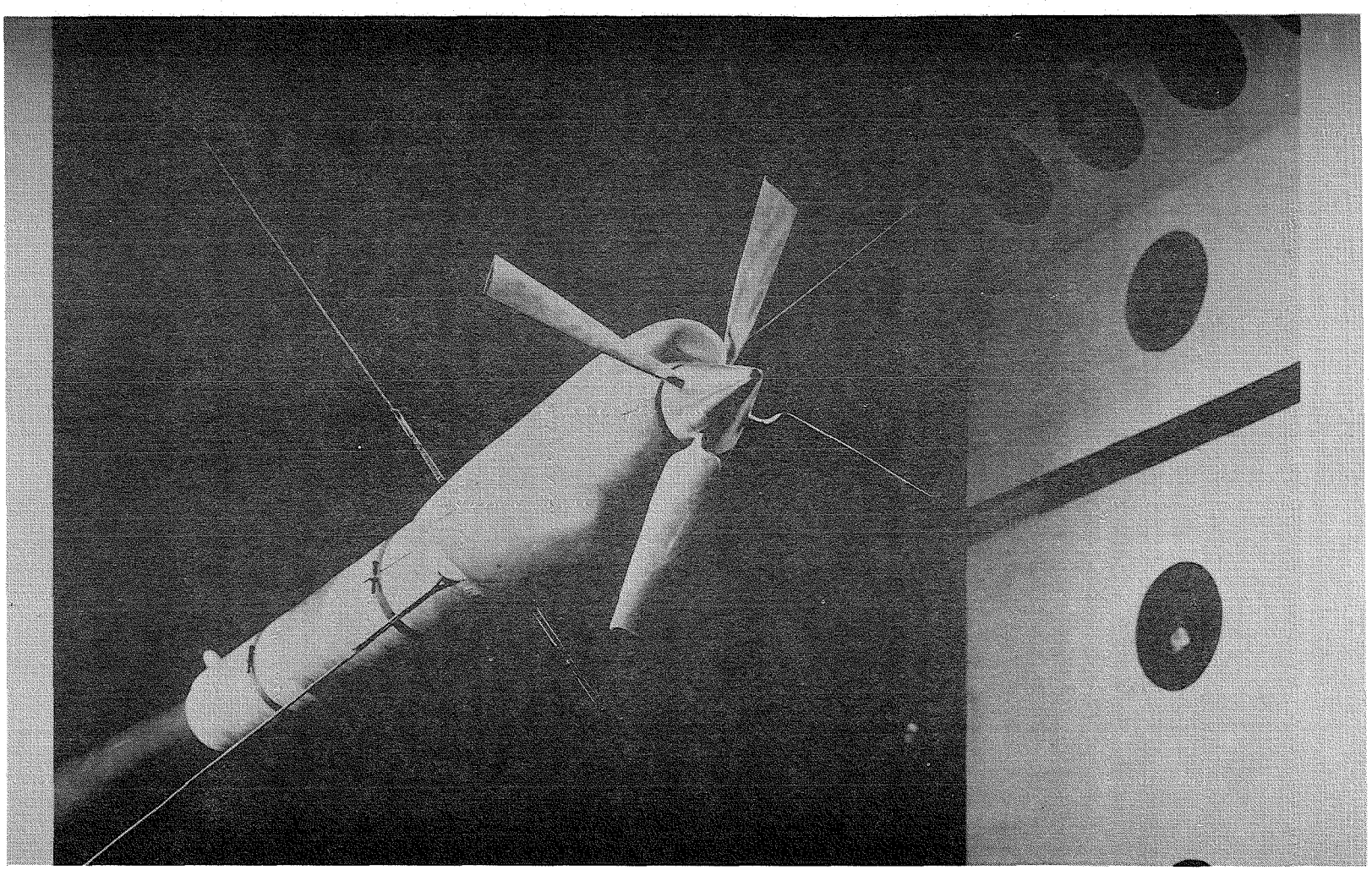

NASA
L-61-6611

Figure 4.- Model used for measuring stability boundaries and aerodynamic derivatives (system 1).

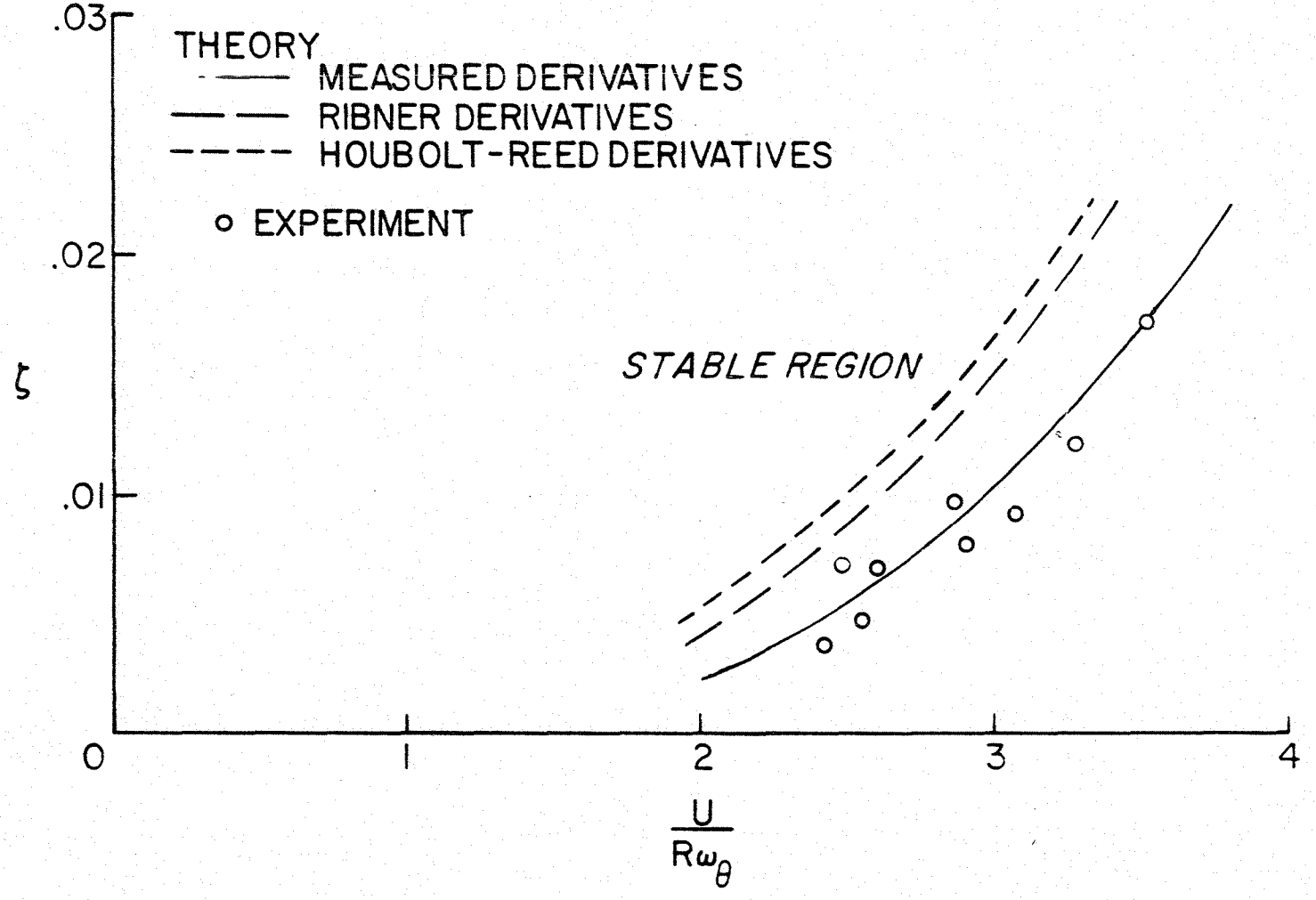

Figure 5.- Comparison of theoretical and experimental whirl flutter boundaries (system 1, J = 2.66).

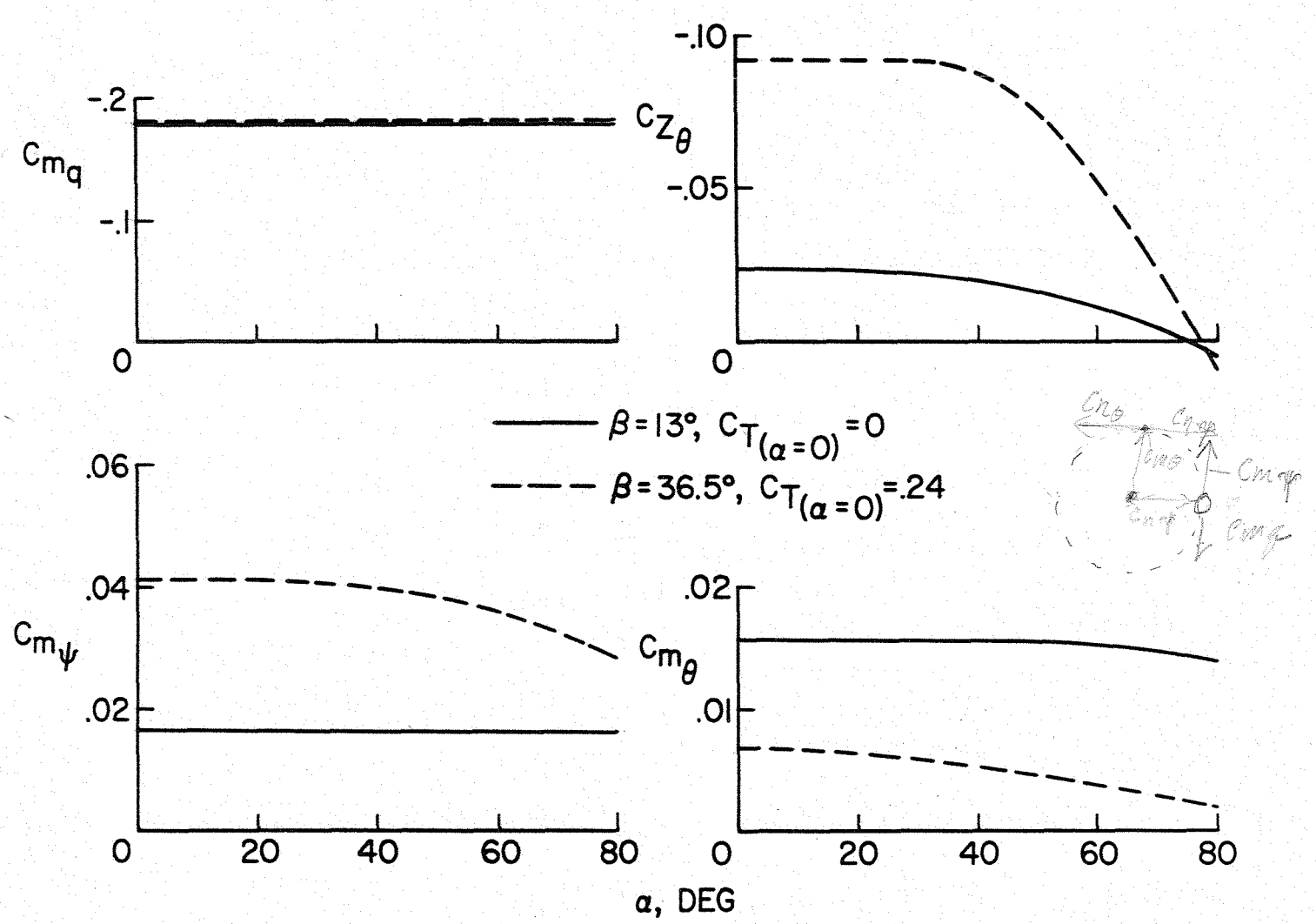

(a) Effect of angle of attack, J = 0.75.

NASA

Figure 6.- Propeller aerodynamic derivatives used in analysis of transition maneuvers for system 2.

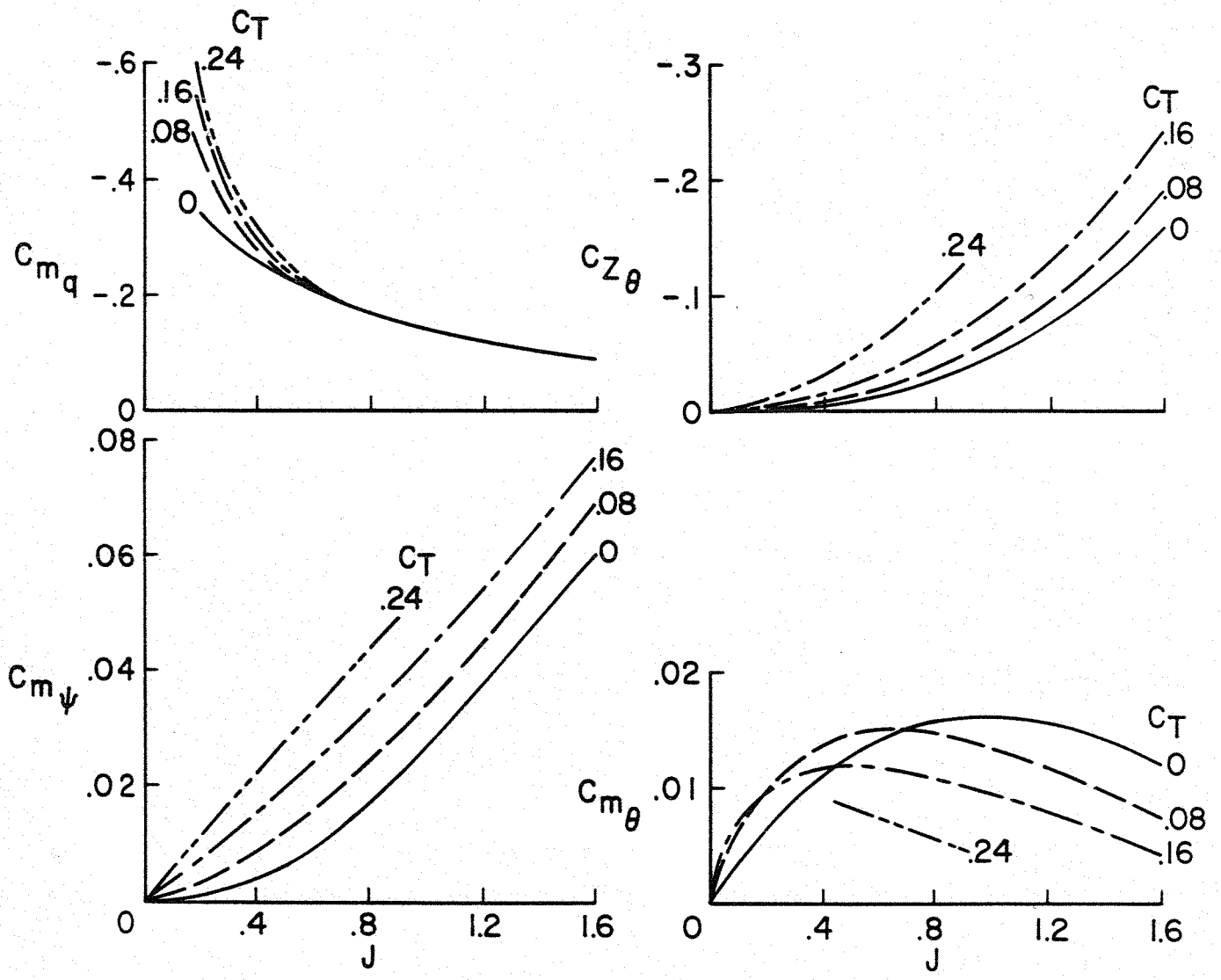

(b) Effect of thrust coefficient for angles of attack less than 30°. NASA

Figure 6.- Concluded.

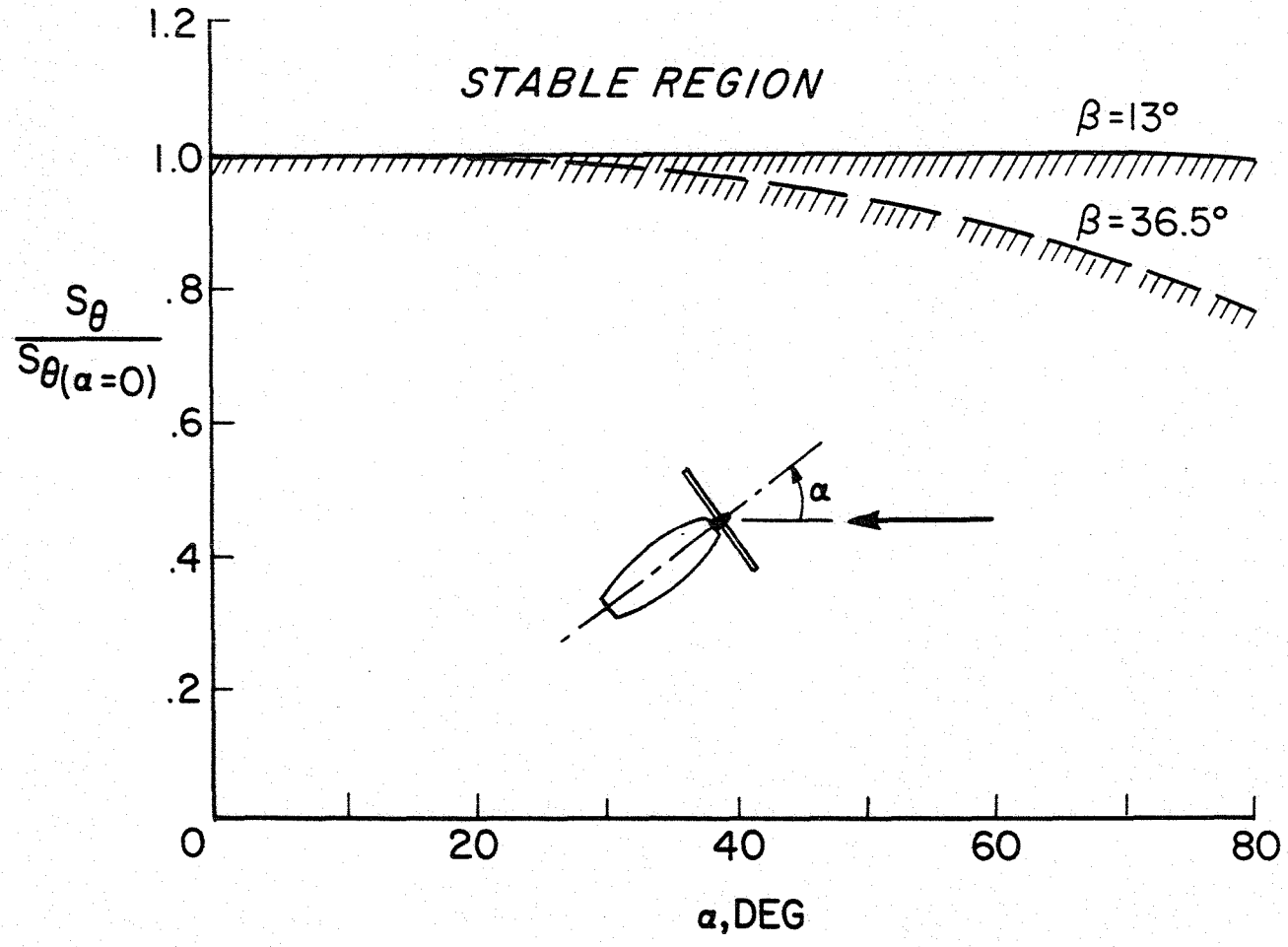

NASA

Figure 7.- Effect of angle of attack at constant blade angle (system 2, $J = 0.75$, $\zeta = 0.05$).

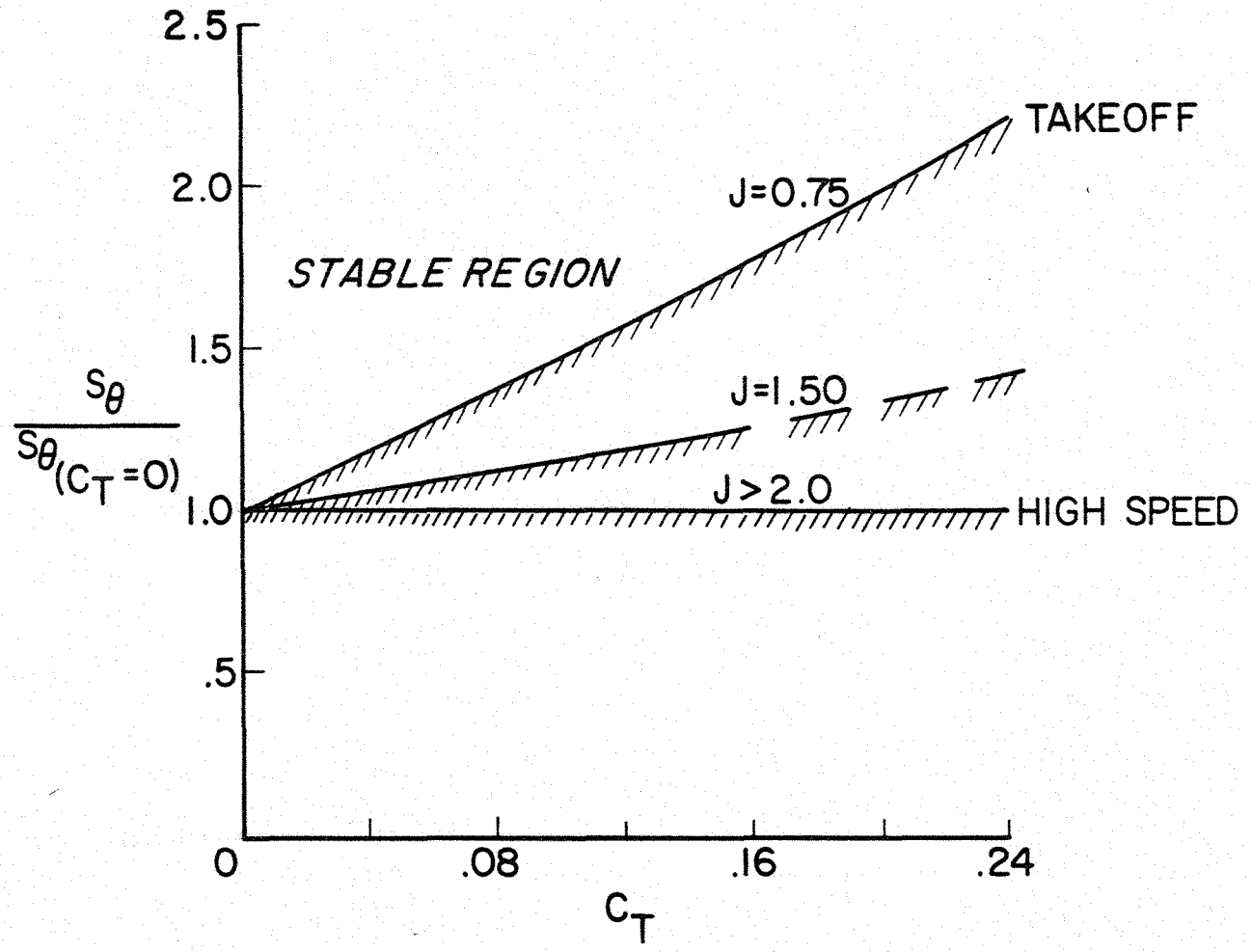

NASA

Figure 8.- Effect of thrust coefficient (system 2, $\zeta = 0.05$, $\alpha = 0$).

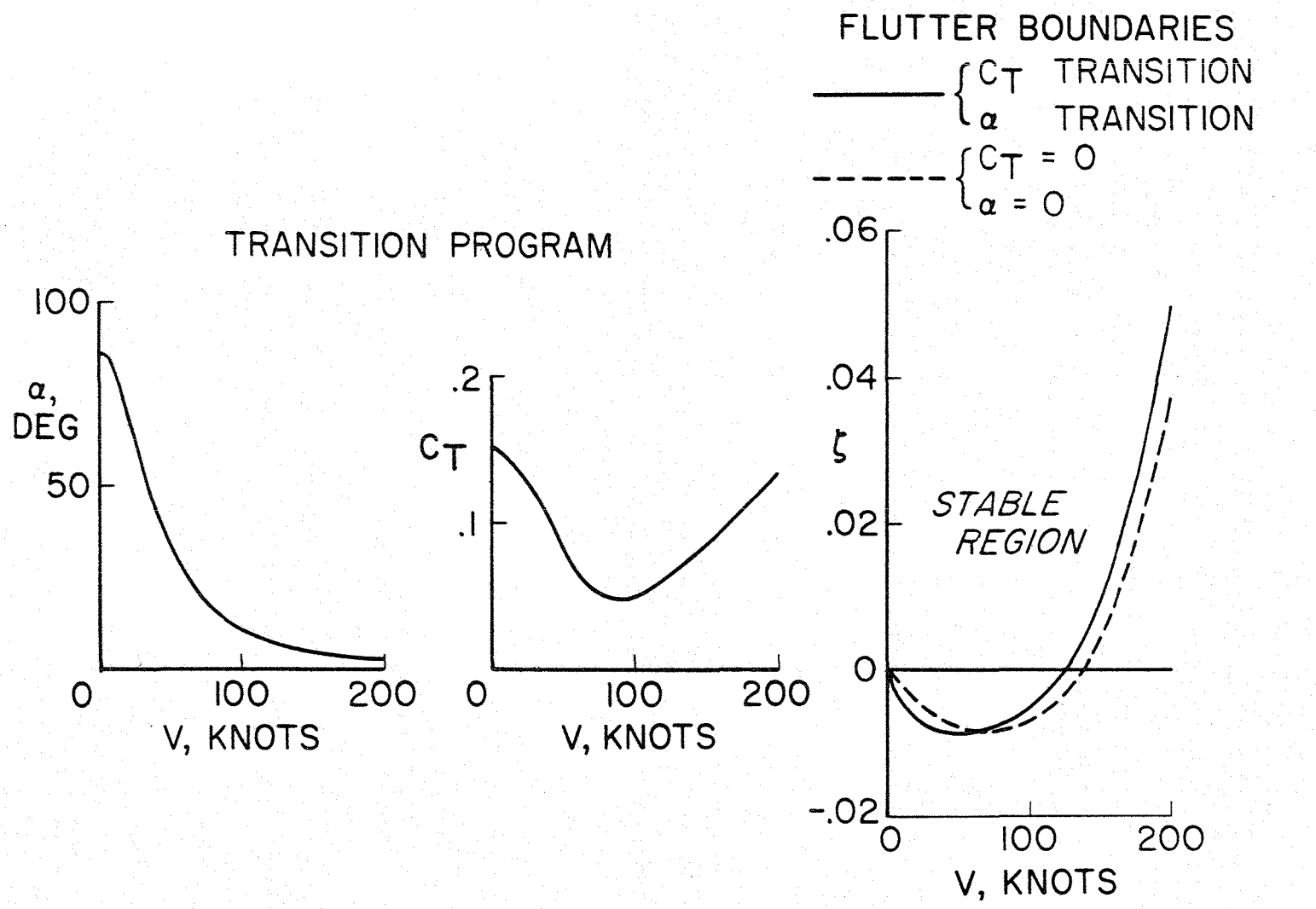

NASA

Figure 9.- Effect of transition program (system 2, $0 \leqq J \leqq 1.5$).

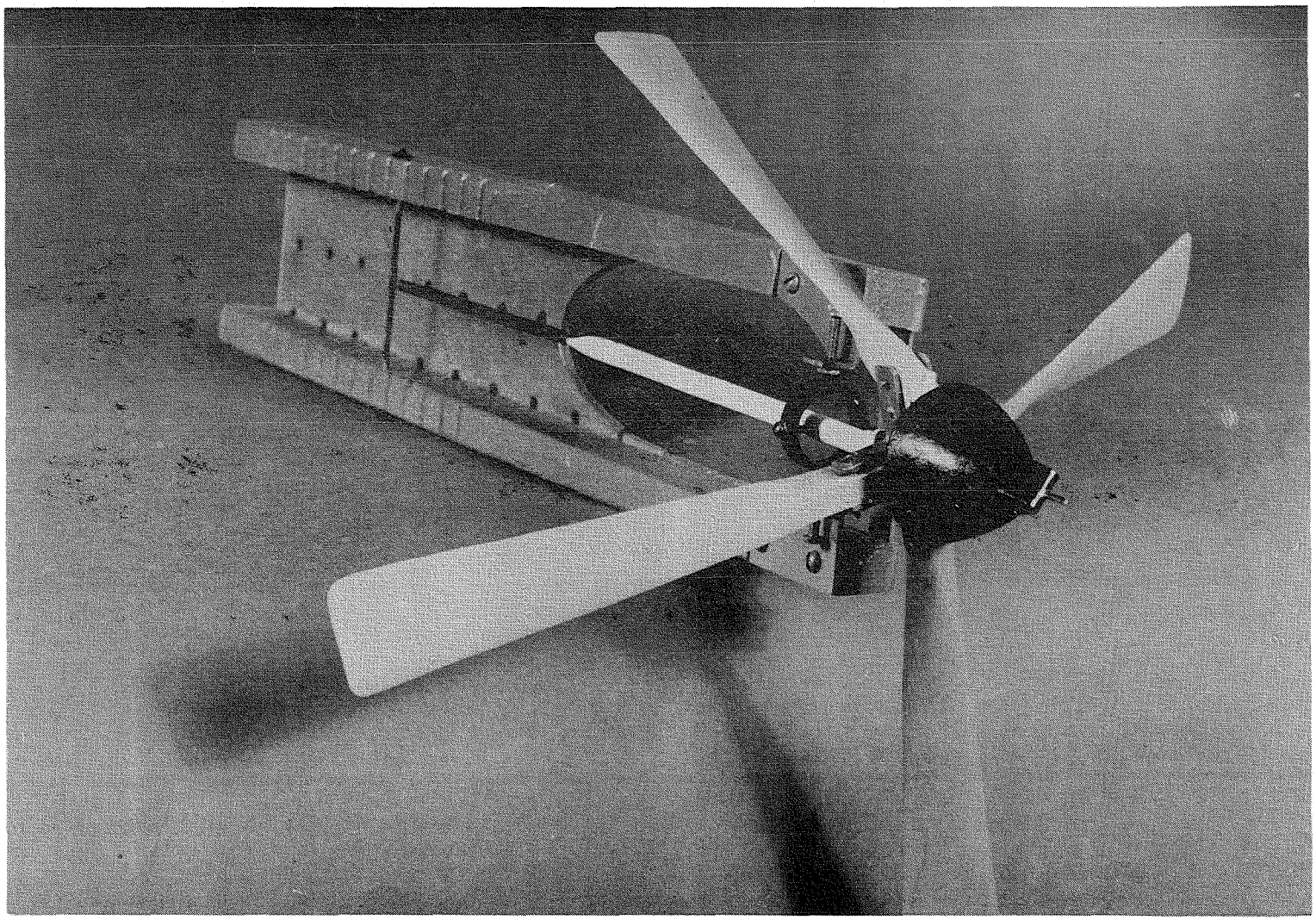

NASA
L-63-247

Figure 10.- Flapping blade propeller whirl model (system 3).

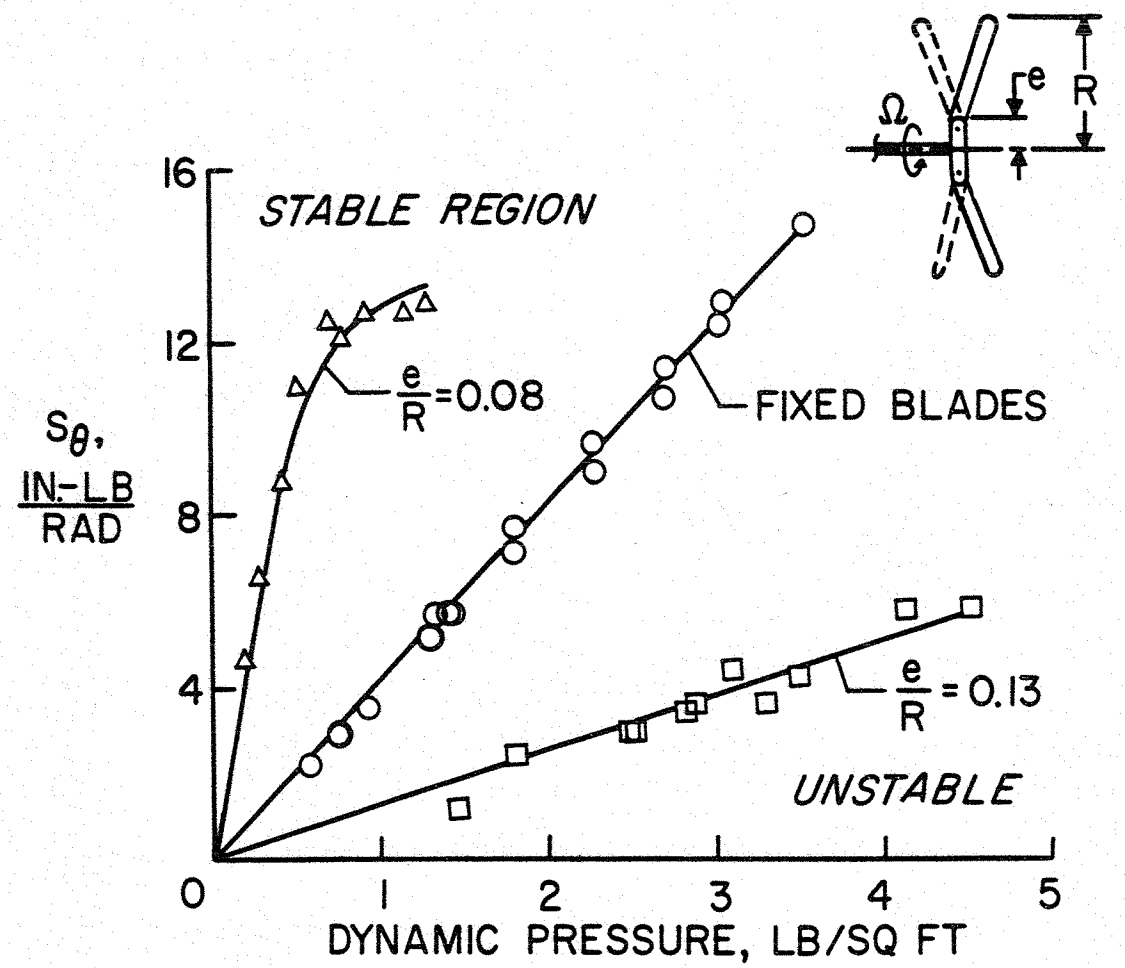

NASA

Figure 11.- Effect of flapping hinges (system 3).

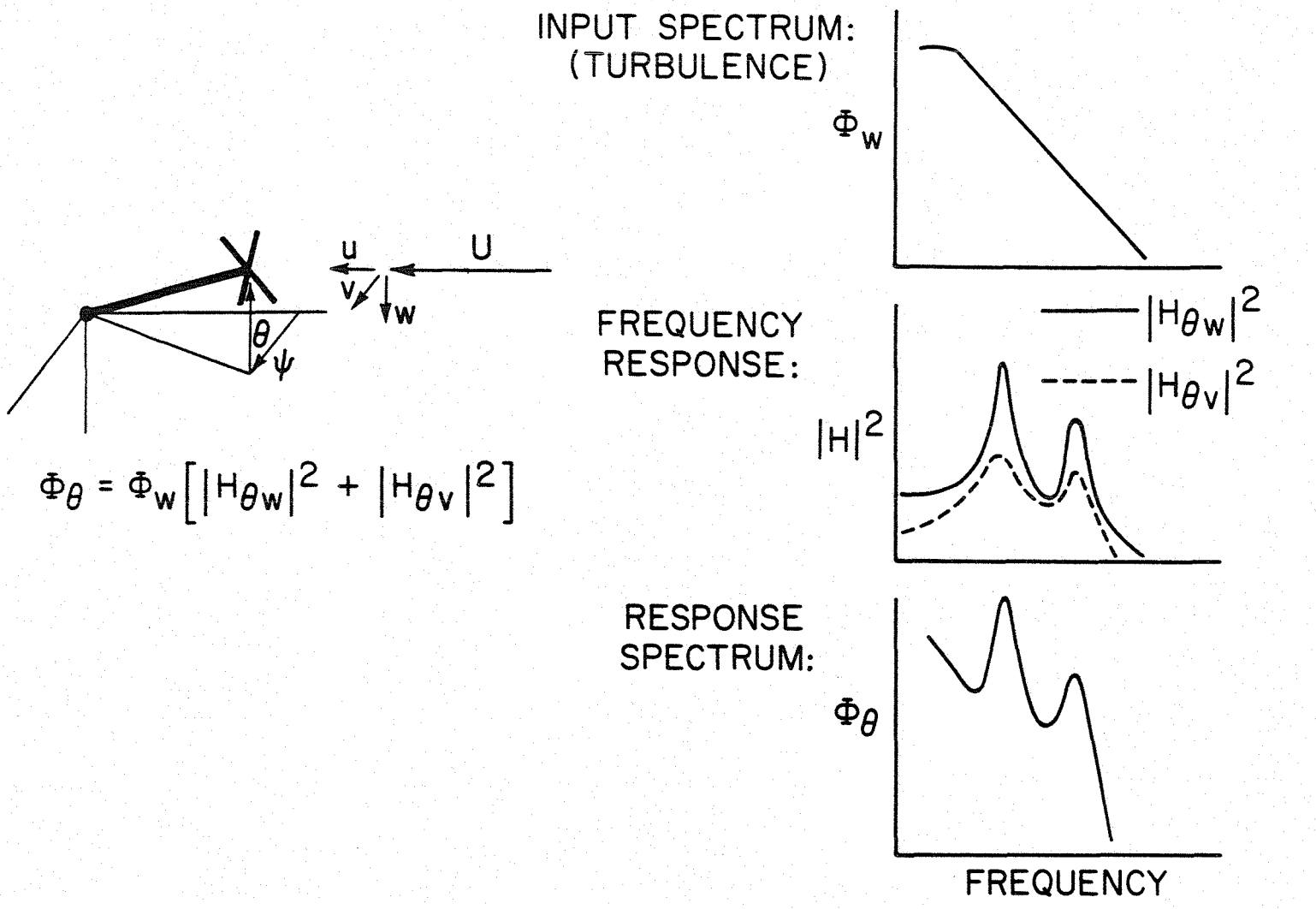

NASA

Figure 12.- Response of propeller system to random turbulence.

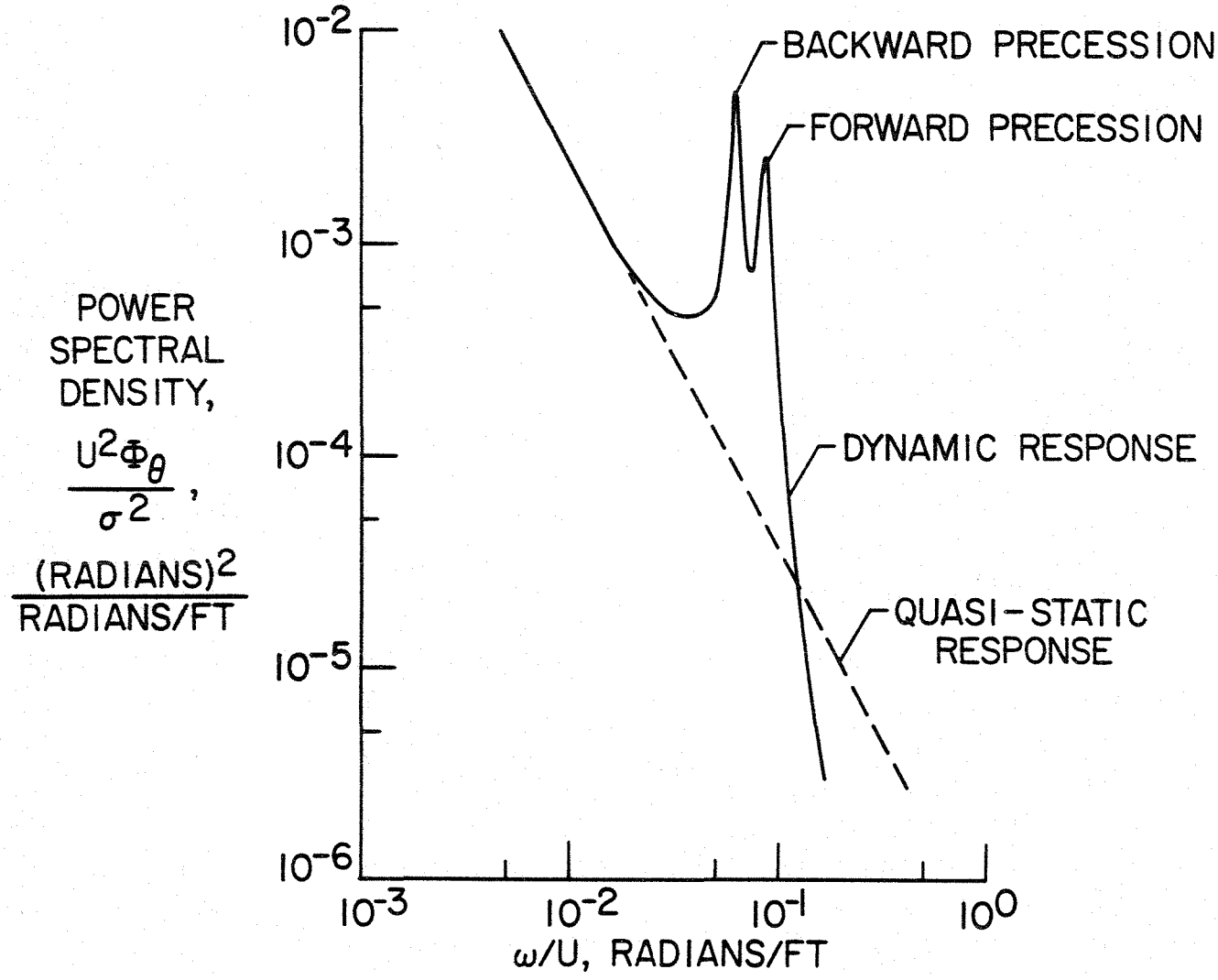

NASA

Figure 13.- Pitch angle response to atmospheric turbulence $\left(\text{system 1, } \zeta = 0.05, \frac{U}{R\omega_\theta} = 2.0, \ J = 2.66\right)$.